Vacuum Ultraviolet Laser-Induced Fluorescence Detection of O(^1S) Atom Produced in the 193 nm Photolysis of Ozone

Kenshi Takahashi,* Tomoki Nakayama, and Yutaka Matsumi

Solar-Terrestrial Environment Laboratory and Graduate School of Science, Nagoya University, Honohara 3−13, Toyokawa, Aichi, 442-8507, Japan

Received: March 18, 2003; In Final Form: August 19, 2003

The O($2p^1S$) atoms produced in the photolysis of O_3 have been detected by a technique of laser-induced fluorescence spectroscopy with the tunable vacuum ultraviolet (VUV) laser radiation around 121.76 nm. The quantum yield value for O(^1S) formation is determined to be $(2.5 \pm 1.1) \times 10^{-3}$ in the 193 nm photolysis of O_3, which is determined by comparing the VUV laser-induced fluorescence intensities of the O($3s^1P_1 - 2p^1S_0$) transition with those of the H($2p^2P_j \leftarrow 1s^2S$) transition at 121.56 nm of the H atoms generated from the photolysis of HCl at 193 nm. The O(^1S) detection technique used in this study is very sensitive, and the detection limit is estimated to be 1×10^9 atoms cm^{-3}. The contribution for the OH radical production from the reaction of H_2O with O(^1S) produced in the UV photolysis of O_3 relative to that from the O(^1D) + H_2O reaction has been estimated as a function of altitude in the stratosphere, using the photolytic O(^1S) quantum yield value obtained in this study and the O(^1S) reaction rate coefficients reported previously. The maximum contribution of the O(^1S) reaction to OH production rate is a 14% fraction of that from the O(^1D) reaction at 40 km altitude at mid-latitudes, assuming the spin-forbidden dissociation process, O(^1S) + $O_2(X^3\Sigma_g^-)$, for the formation of O(^1S) in the photolysis of ozone. Importance of precise measurements of the temperature-dependent reaction rates for O(^1S) has been suggested.

Introduction

Photodissociation reaction of ozone has been extensively studied because of its importance for understanding the photochemical processes of the Earth's atmosphere.[1] The various pathways for ozone photolysis are listed in Table 1 along with their thermochemical threshold wavelengths.[2] The ozone molecule has huge absorption cross sections in the ultraviolet region between 200 and 300 nm.[3,4] The absorption spectrum reported by Malicet et al.[4] is shown in Figure 1. The following two spin-allowed dissociation channels have been believed to be dominant in the photolysis of O_3 in this absorption band:

$$O_3 + h\nu \rightarrow O(^3P) + O_2(X^3\Sigma_g^-) \quad (1)$$

$$O_3 + h\nu \rightarrow O(^1D) + O_2(a^1\Delta_g) \quad (2)$$

At 193 nm, however, 10 dissociation channels are energetically available (Table 1), which are the combinations of the O atomic states (^3P, ^1D, and ^1S) and the O_2 molecular states ($X^3\Sigma_g^-$, $a^1\Delta_g$, $b^1\Sigma_g^+$and $A^3\Sigma_u^+$). The dissociation processes in the photolysis of O_3 at 193 nm have been investigated by several experimental studies. Stranges et al.[5] photolyzed ozone molecular beam at 193 nm and measured the kinetic energy release and recoil anisotropy of atomic oxygen fragments. They reported the product branching ratios of 16.8 ± 1.5%, 45.5 ± 2.5%, 23.3 ± 2.0%, 7.7 ± 0.6%, and 2.0 ± 0.2% for O(^3P) + $O_2(X^3\Sigma_g^-)$, O(^1D) + $O_2(a^1\Delta_g)$, O(^1D) + $O_2(b^1\Sigma_g^+)$, O(^3P) + $O_2(X^3\Sigma_g^-$, vibrationally hot), and 3O(^3P), respectively, from the analysis of the translational energy distributions of oxygen atoms detected by an electron bombardment quadrapole mass spectrometer with an angle resolved time-of-flight technique. Turnipseed et al.[6] studied the photodissociation reaction of O_3 at both 222 and 193 nm by means of the resonance fluorescence detection of O(^3P) atoms with an atomic resonance lamp. They reported the quantum yields for O(^3P) and O(^1D) formation from 193 nm photolysis to be 0.57 ± 0.14 and 0.46 ± 0.29, respectively, and they also estimated the formation yield of $O_2(b^1\Sigma_g^+)$ to be 0.50 ± 0.38. Lee et al.[7] used the synchrotron radiation to photolyze O_3 molecules at 170−240 nm and tried to detect the O(^1S) atoms by observation of the emission that was associated with the O($^1S \rightarrow {}^1D$) forbidden transition around 557.7 nm with

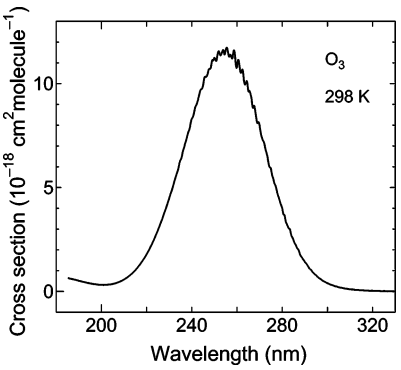

Figure 1. Absorption spectrum of O_3 in the ultraviolet region at 298 K, in which the cross-section data were taken from ref 4.

TABLE 1: Thermochemical Threshold Wavelengths for Photodissociation Pathways of O_3, in Units of nm

	$O_2(X^3\Sigma_g^-)$	$O_2(a^1\Delta_g)$	$O_2(b^1\Sigma_g^+)$	$O_2(A^3\Sigma_u^+)$	$O_2(B^3\Sigma_u^-)$	$2O(^3P)$
O(^3P)	1180	590	460	230	170	198
O(^1D)	410	310	260	167	150	
O(^1S)	234	196	179	129	108	

* Author to whom correspondence should be adressed. E-mail: kent@stelab.nagoya-u.ac.jp.

10.1021/jp0346864 CCC: $25.00 © 2003 American Chemical Society
Published on Web 10/11/2003

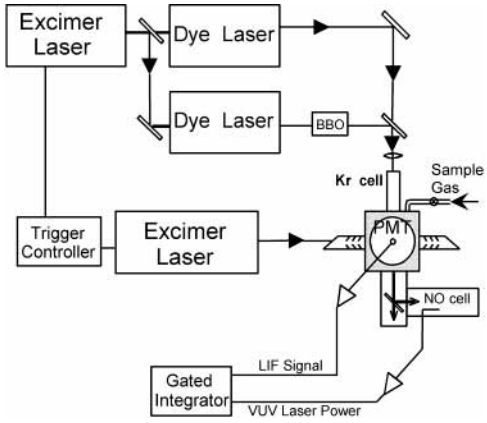

Figure 2. Schematic diagram of the experimental setup for the detection of O(^1S) atoms in the photolysis of ozone with the VUV-LIF technique.

an emission enhancement technique by the formation of XeO excimer. Because they did not observe the emission, they reported the upper limit value of the quantum yield for O(^1S) formation ($\leq$0.1%). Takahashi et al.[8] employed the laser-induced fluorescence (LIF) detection of O(^1D) and O(^3P) fragments from the photolysis of O_3 at 193 nm. The kinetic energy distributions and recoil anisotropies of both nascent fragments were obtained by measuring the Doppler profiles, and dynamics of the UV photodissociation of O_3 were studied.

The formation of O(^1S) in the stratosphere such as the photolysis of ozone can be an important source of OH radicals, because the reaction rate of O(^1S) with H_2O is very fast, while the quenching rates of O(^1S) with N_2 and O_2 are slow. The formation of O(^1S) in the upper atmosphere around 90−100 km is the source of the auroral emission and nightglow at 557.7 nm, which corresponds to the spin-forbidden transition O($^1S \rightarrow {}^1D$). The mechanism of the formation of O(^1S) in the upper atmosphere is still controversial.[9] A new high-sensitive direct detection technique for O(^1S) atoms using a vacuum ultraviolet (VUV) laser system developed in this study will provide a powerful tool for studies on the atmospheric processes concerning the O(^1S) atoms.

In this paper, the O(^1S) formation in the 193 nm photolysis of ozone has been reported. The excitation at 121.76 nm (wavelength in a vacuum), which is resonant to the electronic transition of O($3s^1P_1 - 2p^1S_0$), has been achieved by tunable vacuum UV laser radiation, and the subsequent VUV fluorescence at the same wavelength has been directly detected by a solar-blind photomultiplier. The quantum yield measurements have been made by comparing the VUV-LIF signal intensity of O(^1S) with the that of H(^2S) atom produced in the 193 nm photolysis of HCl, in which the H atom fluorescence has been detected by the same VUV-LIF method at 121.56 nm.

Experimental Section

The O(^1S) atoms produced from O_3 photolysis at 193 nm were quantum-state selectively probed by a technique of VUV-LIF method at 121.76 nm, which is associated with the electronic O($3s^1P_0 - 2p^1S$) transition. Figure 2 shows a schematic diagram of the experimental setup used in this study. The VUV laser around 121.76 nm was generated by four-wave difference frequency mixing ($2\omega_1 - \omega_2$) in Kr/Ar gas mixture.[10] Two dye lasers (Lambda Physik, Scanmate 2E and FL3002E) were simultaneously pumped by an XeCl excimer laser (Lambda Physik, Compex 201). The output from one dye laser was frequency-doubled by a BBO crystal to generate UV laser at 212.56 nm, which was two-photon resonant with Kr $5p[1/2]_0$. The other dye laser output was tuned around 840 nm. The typical pulse energies were 0.3 and 2 mJ for UV and near-IR output, respectively. Laser beams were carefully overlapped using a dichloic mirror and focused into the Kr/Ar containing cell. The generated VUV laser light was introduced into a reaction chamber through a LiF window that was used to separate the Kr/Ar cell and the reaction chamber. A part of the incident VUV light was reflected by another thin LiF plate held in the cell after the photodissociation region and led into a nitric oxide (NO) containing cell. The relative intensity of VUV laser light was monitored by measuring the photoionization current from NO. Typical NO gas pressure was 2−3 Torr.

With the same experimental setup, the tunable VUV laser radiation around 121.56 nm (Lyman-α) was also obtained by tuning the near-IR laser wavelength around 845 nm. The wavelength tunability of the VUV laser is an essential part of this study to determine the quantum yield for O(^1S) production in the 193 nm photolysis of O_3. By comparing the LIF signal intensities for O(^1S) and those for H atom produced in the 193 nm photolysis of HCl, we could estimate the O(^1S) quantum yield value.

The VUV laser line width was estimated to be 0.64 cm^{-1} full-width-at-half-maximum (fwhm) with a Gaussian shape. The line width was estimated by measurement of the Doppler profile of H atom from HCl photolysis at 193 nm, when 2 Torr of He was added to relax translational excitation of the H atom fragments and the time delay between the 193 nm laser and VUV laser pulses was 20 μs. The time delay between the dissociation and probe laser pulses was controlled by a digital delay generator (Stanford Research Systems, DG535).

The VUV-LIF signal of both O(^1S) and H atoms was detected by a solar-blind photomultiplier tube (EMR, 541J-08−17). The three axes for the LIF observation direction, photolysis, and probe laser beam propagation directions are orthogonal to each other. The direction of the fluorescence detection is perpendicular to the electric vector of the VUV probe laser. The output of the photomultiplier was preamplified and averaged over 10 laser pulses using a gated integrator (Stanford Research Systems, SR-250) and then stored on a personal computer.

The reaction cell (80 × 80 × 80 mm) was evacuated by a rotary pump (330 L/min) through a liquid N_2 trap. The pressure in the reaction chamber was measured by a capacitance manometer (MKS, Baratron). Ozone was prepared by passing ultrapure O_2 (99.9995%) through an ozonizer. During the experiments, ozone was supplied to the reaction chamber through glass tubing and a poly-tetrafluoroethylene needle valve with He buffer gas. The total pressure of the gas mixture in the cell was 800−900 mTorr, while the typical partial pressure of O_3 in the reaction cell was 20−30 mTorr. The partial pressure of O_3 was determined by the absorption measurements at 253.7 nm with a mercury resonance lamp and 30 cm path length absorption cell, for which the photoabsorption cross section of at 253.7 nm is known (1.13×10^{-17} cm^2 $molecule^{-1}$).[4] For HCl photolysis, a gas mixture of HCl/Ar (1.43% of HCl in Ar) was used, and the total pressure in the reaction cell was 250−410 mTorr. While scanning the VUV laser wavelength for O(^1S) or H(^2S) atom detections, the reactants' pressure in the cell was kept constant.

Results

Figure 3 shows the fluorescence excitation spectra for O(^1S) and H(^2S) atoms produced in the 193 nm photolysis of O_3 and HCl, respectively. The atomic line profiles of the O($3s^1P_1 \leftarrow$

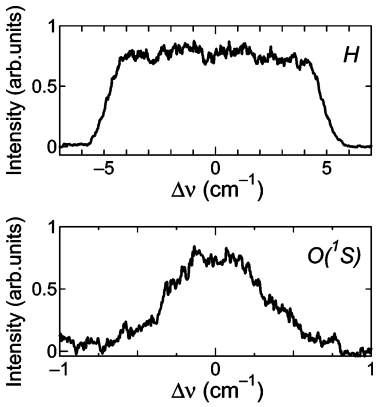

Figure 3. The fluorescence excitation spectra of O(^1S) produced from the photolysis of O_3 at 193 nm and H atoms from HCl at 193 nm, in which the VUV probe laser wavelength was scanned over the Doppler profiles of each fragments. The delay time between the photolysis and probe laser pulses was 150 ns. The partial pressures of O_3 and HCl in the reaction cell was 20 and 4 mTorr, respectively.

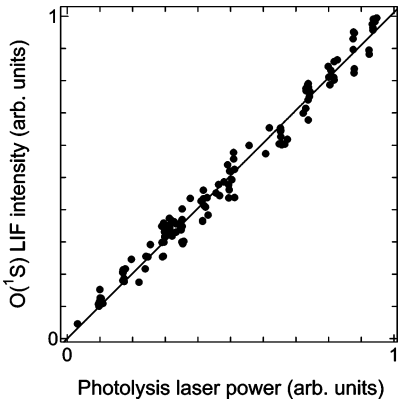

Figure 4. LIF signal intensity for O(^1S) versus the photolysis laser power. The photolysis laser power was changed while monitoring the O(^1S) LIF signal at 121.76 nm. The time delay between the photolysis and probe laser pulses was 150 ns, and the pressure of O_3 in the reaction cell was kept to be 20 mTorr.

$2p^1S_0$) transition were directly detected by VUV-LIF method around 121.76 nm, while those of the H($2p^2P_j \leftarrow 1s^2S$) transition were detected at 121.56 nm. The time delay between the photolysis and probe laser pulses was 150 ns. The absolute quantum yield for O(^1S) formation, $\Phi_{O(1S)}$, was obtained by the following equation:

$$\Phi_{O(1S)} = \frac{A_{O(1S)} I_H f_H \sigma_{HCl}[HCl] \Phi_H \phi_H}{A_H I_{O(1S)} f_{O(1S)} \sigma_{O3}[O_3] \phi_{O(1S)}} \quad (3)$$

where $A_{O(1S)}$ and A_H are the peak areas of the fluorescence excitation spectra of O(^1S) atoms in the photolysis of O_3 and H atoms in the photolysis of HCl, respectively, $I_{O(1S)}$ and I_H are the probe laser intensities at the resonance wavelengths of O(^1S) (121.76 nm) and H atoms (121.56 nm), respectively, Φ_H is the production quantum yield of H atoms in the photolysis of HCl, σ_{O3} and σ_{HCl} are the photoabsoption cross sections of O_3 and HCl, respectively, at 193 nm, $f_{O(1S)}$ and f_H are the transition probabilities for O($3s^1P_1 \leftarrow 2p^1S_0$) and H($2p^2P_j \leftarrow 1s^2S$) optical excitation, respectively, and $\phi_{O(1S)}$ and ϕ_H indicate the detection efficiencies of the resonance fluorescence from the excited states, O($3s^1P_1$) and H($2p^2P_j$), respectively, which are prepared by the VUV laser irradiation. The 193 nm photolysis of HCl generates H atoms with a photolysis quantum yield of unity, that is $\Phi_H = 1$. The values of f_H and $f_{O(1S)}$ are taken from the database of NIST.[11] The upper excited state of H($2p^2P_j$) has two spin−orbit components (j =1/2, 3/2), in which the spin−orbit energy separation is reported to be 0.36 cm^{-1}.[11] Because the energy separation is smaller than our VUV laser line width (0.64 cm^{-1}), the two peaks due to the spin−orbit components of H($2p^2P_j$) were not separated in the excitation spectra, and the value of $f_H = 0.416$ is used. The values of σ_{O3} and σ_{HCl} are 4.34×10^{-19} and 8.69×10^{-20} in units of cm^{2}molecule^{-1}, which are reported by Molina and Molina[3] and Sander et al,[12] respectively. The values of $A_{O(1S)}$ and A_H are obtained by integrating the atomic line shapes in the fluorescence excitation spectra measured for O(^1S) and H atoms, respectively. The probe laser intensities, $I_{O(1S)}$ and I_H, are obtained from the signal intensity of the nitric oxide photoionization cell. The photoionization efficiencies of NO molecule used in the relative intensity measurements of the probe laser at 121.76 and 121.56 nm are also taken into account.[13,14]

The detection efficiency of the PMT system is assumed to be constant between the resonance fluorescence wavelengths of O($3s^1P_1 - 2p^1S_0$) and H($2p^2Pj - 1s^2S$) at 121.76 and 121.56 nm, respectively, because the difference of the wavelengths is very small. The collisional quenching of the VUV fluorescence from the electronically excited states, O($3s^1P_1$) and H($2p^2P_j$), can be ignored under our experimental conditions, because the total pressures used in the experiments are less than 1 Torr, and the radiative decay lifetimes of the excited states are less than several nanoseconds. However, the electronic state O($3s^1P_1$), which is prepared by the VUV laser excitation at 121.76 nm, emits the two transition lines, $3p^1P_1 \rightarrow 2p^1S_0$ at 121.76 nm and $3p^1P_1 \rightarrow 2p^1D_2$ at 99.95 nm. The latter transition is not detected by the photomultiplier through a lithium fluoride (LiF) window. The A-value for the O($3p^1P_1 \rightarrow 2p^1S_0$) transition is $A_1 = 2.06 \times 10^8$ sec^{-1} and that for O($3p^1P_1 \rightarrow 2p^1D_2$) is $A_2 = 5.06 \times 10^8$ sec^{-1}. We used the relative values of the detection efficiencies as $\phi_{O(1S)} = A_1/(A_1 + A_2)$ and $\phi_H = 1$. In the experiments, the O(^1S) detection and the H detection were alternatively performed by changing the reactants and probe laser wavelengths. Intensity variation of the 193 nm laser light was small (<5%) through the alternative measurements. The experimental runs were performed six times repeatedly to record the fluorescence excitation spectra. Thus, $\Phi_{O(1S)} = (2.5 \pm 1.1) \times 10^{-3}$ was obtained, where the quoted error was the 2σ statistical uncertainties of the experimental data.

Checks were made to ensure that the O(^1S) LIF signal scaled linearly with the intensity of the 193 nm photodissociation laser pulse, as shown in Figure 4. We also checked that neither the O(^1S) nor H atoms' signal was detected without 193 nm photolysis light. Therefore, these observations indicate that multiphoton absorption processes at 193 nm or dissociation of parent molecules at the probe laser wavelengths were safely ignored in this work.

Under our experimental conditions of low gas pressures and short delay time (150 ns), chemical loss of O(^1S) and H atoms through secondary reactions can be safely ignored. For instance, the room-temperature reaction rate constants for $H + HCl \rightarrow H_2 + Cl$[15] and O($^1S$) + $O_2 \rightarrow$ products[16] were reported to be 2.74×10^{-13} and 2.6×10^{-13} in units of cm^3 mol^{-1} s^{-1}, respectively.

Discussion

In the stratosphere, the photolysis of ozone molecules around 185−210 nm can take place fairly, because this wavelength range corresponds to the "atmospheric window" due to the edge of the overlapping of O_2 and O_3 absorption. This is the first

report on determination of the quantum yield of the O(^1S) atoms produced in the 193 nm photolysis of O_3. The $\Phi_{O(1S)}$ value obtained in this study suggests that the dissociation pathway(s) to produce the O(^1S) atom in the 193 nm photolysis of ozone is a minor process. Lee et al.[7] observed the XeO exicimer emission around 557.7 nm, in the photolysis of the gas mixture of N_2O and Xe with irradiation of 134.7 nm synchrotron radiation, which indicated the formation of O(^1S) in the photolysis of N_2O at 134.7 nm. However, they did not detect the emission around 557.7 nm from the gas mixture of O_3, N_2O, and Xe with the irradiation of the synchrotron radiation between 170 and 240 nm.[7] They presented the upper limit value for O(^1S) formation in the O_3 photolysis between 170 and 240 nm to be 0.1%. The O(^1S) yield value, $\Phi_{O(1S)} = (2.5 \pm 1.1) \times 10^{-3}$, which is obtained in this study for the photolysis of O_3 at 193 nm, is a little larger than the upper limit value reported by Lee et al.[7]

There are two energetically available pathways for O(^1S) formation in the 193 nm photolysis of O_3 (Table 1), namely

$$O_3 + h\nu \rightarrow O(^1S) + O_2(X^3\Sigma_g^-) \quad (4)$$

$$O_3 + h\nu \rightarrow O(^1S) + O_2(a^1\Delta_g) \quad (5)$$

The former is a spin-forbidden channel, while the latter is a spin-allowed. In our experiments, the spectral resolution for the O($3p^1P_1 \rightarrow 2p^1S_0$) transition line in the excitation spectra is not high enough to detect the maximum Doppler broadening due to the excess energy to distinguish processes (4) and (5), because the energy difference between the $O_2(X^3\Sigma_g^-)$ and $O_2(a^1\Delta_g)$ states is small. Moreover, the translational energy of O(^1S) can be partley relaxed under our experimental conditions.

Turnipseed et al.[6] reported the formation quantum yields of the O(^1D) and O(^3P) in the photolysis of O_3 at 193 nm, which were 0.46 ± 0.29 for O(^1D) and 0.57 ± 0.14 for O(^3P), using a resonance fluorescence detection technique with an oxygen lamp at 130 nm. They also estimated the formation yield of $O_2(b^1\Sigma_g^+)$ was 0.50 ± 0.38. Their results for O(^3P) and O(^1D) and the small yield of O(^1S) obtained in this study indicate that the predominant photodissociation processes of O_3 in the "atmospheric window" region (185−210 nm) may be O(^1D) + $O_2(b^1\Sigma_g^+)/O_2(a^1\Delta_g)$ and O(^3P) + $O_2(X^3\Sigma_g^-)$.

The O(^1S) atoms do not react with N_2 or O_2 efficiently, and the reaction rates are relatively small, with the following room-temeprature rate coefficients:[16]

$$O(^1S) + N_2 \rightarrow O(^1D \text{ or } ^3P) + N_2 \qquad k_6 < 5 \times 10^{-17}\ \text{cm}^3\ \text{molecule}^{-1}\ \text{s}^{-1} \quad (6)$$

$$O(^1S) + O_2 \rightarrow O(^1D \text{ or } ^3P) + O_2 \qquad k_7 = 2.6 \times 10^{-13}\ \text{cm}^3\ \text{molecule}^{-1}\ \text{s}^{-1} \quad (7)$$

while the reaction rate with H_2O is very large[17]

$$O(^1S) + H_2O \rightarrow \text{products} \qquad k_8 = 5.0 \times 10^{-10}\ \text{cm}^3\ \text{molecule}^{-1}\ \text{s}^{-1} \quad (8)$$

This behavior of the O(^1S) reaction processes is quite different from that of the O(^1D) reaction processes. The de-excitation processes of O(^1D) by N_2 and O_2 are fast, with the room-temeprature rate coefficients of 2.6×10^{-11} and 4.0×10^{-11} in units of cm^3 molecule^{-1} s^{-1}, respectively.[12] The photolytic formation of O(^1S) in the upper atmosphere provides an OH source because the branching for OH formation in reaction (8) is reported to be 0.61.[17] We have roughly estimated the importance of the contribution of O(^1S) + H_2O to the OH production at 40 km altitude in mid-latitudes at noon. The production rate of OH radical from the reactions of O(^1S) + H_2O or O(^1D) + H_2O, R_{OH}, is expressed as

$$R_{OH} = \frac{k_{H_2O}[H_2O]Y}{k_{H_2O}[H_2O] + k_{N_2}[N_2] + k_{O_2}[O_2]} \times [O_3]\int_\lambda F(\lambda)\sigma_{O3}(\lambda)\Phi(\lambda)d\lambda \quad (9)$$

where λ is wavelength, $F(\lambda)$ is the solar flux, $\sigma_{O3}(\lambda)$ is the absorption cross section of ozone, Y is the molar yield for OH formation from the O(^{1}D)(=1) or O(^{1}S)(=0.61) reactions, $\Phi(\lambda)$ is the quantum yield of O(^1S) or O(^1D) from the photolysis of ozone at λ, k_{H_2O}, k_{N_2}, and k_{O_2} are the reaction rate constants of O(^1S) or O(^1D) with H_2O, N_2, and O_2, respectively. Hereafter, the OH production rate from the O(^1S) reaction is denoted as R_{OH}^{1S}, while that from the O(^1D) reaction is done as R_{OH}^{1D}. The values of $F(\lambda)$ are calculated using the program presented by Kylling et al.[18] The values of temperature-dependent $\sigma_{O3}(\lambda)$ are taken from the data presented by Molina and Molina.[3] For R_{OH} calculations, the cross sections below 240 nm at 263 K are interpolated from the values reported for 226 and 298 K. For the reaction rate coefficients for O(^1S), the room-temperature values of k_{6-8} are used, because their temperature dependences are unknown. The rate constants for O(^1D) reactions are taken from the NASA/JPL databook.[12] The typical mixing ratio of H_2O vapor is assumed to be 3−5 ppmv at altitudes estimated. The values of the quantum yield of O(^1D) as a function of wavelength is taken from the data by Matsumi et al.[1] (308−328 nm), Takahashi et al.[19] (230−308 nm), and Cooper et al.[20] (221−230 nm). For a range of 193−221 nm, we assumed the linear function using the value of 0.46 at 193 nm presented by Turnipseed et al.[6] and the value at 221 nm of 0.87 by Cooper et al.[20] Below 193 nm, the O(^1D) quantum yield value is assumed to be 0.46.

For wavelength dependence of $\Phi_{O(1S)}(\lambda)$, two different processes of the O(^1S) formation in the photolysis of O_3 have been considered. One is that the O(^1S) atoms are produced through the spin-forbidden dissociation process (4) and $\Phi_{O(1S)}(\lambda)$ is constant at 2.5×10^{-3}, which is obtained at 193 nm in this study, below the channel (4) threshold wavelength of 234 nm. The other is that the O(^1S) atoms are produced through the spin-allowed dissociation process (5) and $\Phi_{O(1S)}(\lambda)$ is constant at 2.5×10^{-3} below the channel (4) threshold wavelength of 196 nm. The O(^1D) and O(^1S) quantum yield values used in the $R_{OH}{}^{1S}$ and $R_{OH}{}^{1D}$ calculations and the action spectra in 2-nm intervals for OH production at 40 km at mid-latitudes are shown in Figure 5. The integrated area of each spectrum shown in the lower panel of Figure 5 corresponds to R_{OH}. The percentage fraction of the OH production from reaction (8) relative to O(^1D) + H_2O, $R_{OH}{}^{1S}/R_{OH}{}^{1D} \times 100$, as a function of altitude between 30 and 70 km at mid-latitudes, is graphically shown in Figure 6. If the O(^1S) atoms are produced from the spin-forbidden channel (4) and the yield is constant at wavelengths below 234 nm, the maximum contribution of reaction O(^1S) + H_2O in the atmospheric OH production relative to the well-established O(^1D) + H_2O reaction appears at 40 km, and the fraction is about 14%. At about 40 km, the atmospheric window region is relatively important in the solar actinic flux penetrated into the atmosphere. If the O(^1S) atoms are produced only from the spin-allowed process (5), the fraction is less than 0.1% at all altitudes estimated, and reaction (8) does not become a significant OH

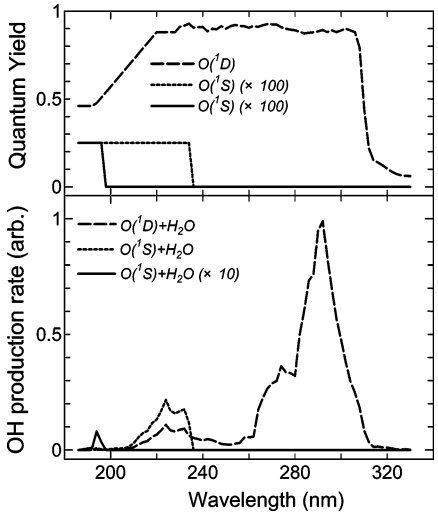

Figure 5. Upper panel: Quantum yield values for $O(^1D)$ (broken line) and $O(^1S)$ (dot and solid lines) atoms formation from the ultlaviolet photolysis of O_3 as a function of wavelength, which are used for calculations of the atmospheric OH production rates through the reactions of $O(^1D)$ and $O(^1S)$ atoms with H_2O vapor. Two different $O(^1S)$ formation processes are assumed for the wavelength-dependent $O(^1S)$ quantum yields; the dotted line indicates the $O(^1S)$ formation through the spin-forbidden process and constant quantum yields below 234 nm, while the solid line indicates the $O(^1S)$ formation through the spin-allowed process and constant quantum yields below 196 nm. Lower panel: Action spectra for the OH production rate at 40 km at mid-latitudes, calculated in 2-nm intervals. Broken line indicates the contribution of $O(^1D) + H_2O$, while dot and solid lines indicate those of $O(^1S) + H_2O$ assuming the spin-forbidden and spin-allowed formation processes, respectively, for the $O(^1S)$ formation from the O_3 photolysis.

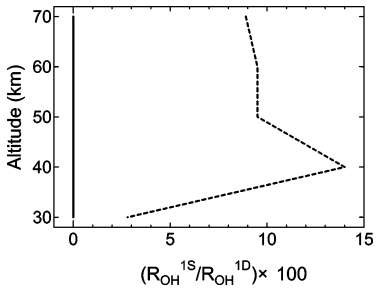

Figure 6. Percentage fraction of the calculated OH production from $O(^1S) + H_2O$ relative to $O(^1D) + H_2O$, $R_{OH}{}^{1S}/R_{OH}{}^{1D} \times 100$, as a function of altitude in the mid-latitudes. Indications of the dotted and solid lines correspond to those in Figure 5, that is, the spin-forbidden formation and the spin-allowed processes, respectively, for the $O(^1S)$ formation in the O_3 photolysis.

source. It should be noted that in these calculations the temperature dependences of the rate coefficients for $O(^1S)$ reactions are not taken into account. The temperature-dependent rate coefficient for reaction (8) has not been investigated yet as far as the authors know, although that for reaction (7) has been reported by Capetanakis et al.[21] If the temperature dependent rate coefficient only for reaction 7 was taken into account, the $R_{OH}{}^{1S}/R_{OH}{}^{1D} \times 100$ value was 25%, on the assumption that $O(^1S)$ is formed via spin-forbidden channel from O_3. The present calculations suggest that it is important for understanding the stratospheric and mesospheric processes to determine the $O(^1S)$ quantum yield values from O_3 photolysis between 193 and 234 nm and the temperature-dependent reaction rate coefficients of $O(^1S)$ with H_2O, N_2 and O_2.

Conway et al.[22] have studied the issue of "HO_x dilemma", that is, the satellite observations indicate the OH densities near 43 km in the stratosphere are about 20% higher than those predicted by standard photochemical theory, while those in the mesosphere (50−80 km) are lower than the theoretical prediction. The main OH formation process around 43 km is thought to be the $O(^1D) + H_2O$ reaction following the ozone photolysis, while that above 60 km altitude is to be the photolysis of H_2O. The new OH production process (8) could provide some solution for the HO_x dilemma, if the $O(^1S)$ atoms were generated by the spin-forbidden photodissociation of ozone channel (4). Other spin-forbidden dissociation processes of $O(^1D) + O_2(X^3\Sigma_g^-)$ and $O(^3P) + O_2(a^1\Delta_g)$ in the photolysis of ozone have been reported at the longer wavelengths (∼325 nm) with the quantum yields of 0.08−0.10.[23−25]

The optical emission of the atomic transition of $O(^1S-{}^1D)$ at 557.7 nm is a spin-forbidden process, and the radiative lifetime is 0.71 s. At high altitudes (90−100 km) the green emission of the $O(^1S-{}^1D)$ transition is observed as nightglow. The formation process of the $O(^1S)$ atoms in the upper atmosphere is still controversial.[9] The $O(^1S)$ atoms for the nightglow have been considered to be formed by a two step scheme

$$O + O + M \rightarrow O_2^* + M \quad (10)$$

$$O + O_2^* \rightarrow O(^1S) + O_2 \quad (11)$$

The electronic state of the intermediate O_2^* for the production of $O(^1S)$ is not well identified. For detection of the $O(^1S)$ atoms in laboratory experiments such as kinetic studies, the $O(^1S \rightarrow {}^1D)$ spin-forbidden emission at 557.7 nm has been observed. The sensitivity of this technique should be low, because the radiation lifetime is very long and most of $O(^1S)$ atoms are quenched. In this study, we have used the VUV laser-induced fluorescence technique to detect the $O(^1S)$ atoms at 121.76 nm. The detection limit for the $O(^1S)$ atoms detected is estimated to be 1×10^9 atoms cm^{-3} under our experimental conditions used in this study. This technique can be useful for the investigations of formation and reaction processes of $O(^1S)$ in the upper atmosphere with laboratory experiments.

Acknowledgment. This work was partly supported by Grant-in-Aid from the Ministry of Education, Culture, Sports, Science and Technology, Japan. This work is also partly supported by Steel Industrial Foundation for the Advancement of Environmental Protection Technology. The authors thank K. Toyota (Frontier research system for global change) for his help in running the radiation calculation program.

References and Notes

(1) Matsumi, Y.; Comes, F. J.; Hancock, G.; Hofzumahaus, A.; Hynes, A. J.; Kawasaki, M.; Ravishankara, A. R. *J. Geophys. Res.* **2002**, *107*, 10.1029/2001JD000510.

(2) Atkinson, R.; Baulch, D. L.; Cox, R. A.; Hampson, R. F., Jr; Kerr, J. A.; Rossi, M. J.; Troe, J. *J. Phys. Chem. Ref. Data* **1997**, *27*, 1329.

(3) Molina, L. T.; Molina, M. J. *J. Geophys. Res*. **1986**, 91, 14501.

(4) Malicet, J.; Daumont, D.; Charbonnier, J.; Parisse, C.; Chakir, A.; Brion, J. *J. Atmos. Chem.* **1995**, *21*, 263.

(5) Stranges, D.; Yang, X.; Chesko, J. D.; Suits, A. G. *J. Chem. Phys.* **1995**, *102*, 6067.

(6) Turnipseed, A. A.; Vaghjiani, G. L.; Gierczak, T.; Thompson, J. E.; Ravishankara, A. R. *J. Chem. Phys.* **1991**, *95*, 3244.

(7) Lee, L. C.; Black, G.; Sharpless, R. L.; Slanger, T. G. *J. Chem. Phys.* **1980**, *73*, 256.

(8) Takahashi, K.; Taniguchi, N.; Matsumi, Y.; Kawasaki, M. *Chem. Phys.* **1998**, *231*, 171.

(9) Wayne, R. P. *Chemistry of Atmospheres*, 3rd Edition; Oxford University Press: New York, 2000.

(10) Marangos, J. P.; Shen, N.; Ma, H.; Hutchinson, M. H. R.; Cornerade, J. P. *J. Opt. Soc. Am.* **1990**, *B7*, 1254.

(11) National Institute for Standard Technology (NIST) Scientific and Technical Databases, Atomic and molecular physics, http://www.nist.gov/srd/atomic.htm.

(12) Sander, S. P.; Friedl, R. R.; DeMore, W. B.; Golden, D. M.; Kurylo, M. J.; Hampson, R. F.; Huie, R. E.; Moortgat, G. K.; Ravishankara, A. R.; Kolb, C. E.; Molina, M. J. *Chemical Kinetics and Photochemical Data for use in Stratospheric Modeling*, Evaluation Number 13; Jet Propulsion Laboratory, 2000.

(13) Ono, Y.; Lin, S. H.; Prest, H. F.; Ng, C. Y.; *J. Chem. Phys.* **1980**, *73*, 4855.

(14) Erman, P.; Karawajczyk, A.; Rachelew-Källine, E.; Strömholm, C. *J. Chem. Phys.* **1995**, *102*, 3064.

(15) Adusei G. Y.; Fontijn, A. *J. Phys. Chem.* **1993**, *97*, 1409.

(16) Okabe, H. *Photochemistry of small molecules*, Wiley-Interscience: New York, 1978.

(17) Slanger, T. G.; Black, G. *J. Chem. Phys.* **1978**, *68*, 989.

(18) Kylling, A.; Stamnes, K.; Tsay, S.-C. *J. Atmos. Chem.* **1995**, *21*, 115.

(19) Takahashi, K.; Hayashi, S.; Matsumi, Y.; Taniguchi, N.; Hayashida, S. *J. Geophys. Res.* **2002**, *107*, 10.1029/2001JD002048.

(20) Cooper, I. A.; Neill, P. J.; Wiesenfeld, J. R. *J. Geophys. Res.* **1993**, *98*, 12795.

(21) Capetanaskis, F. P.; Sondermann, F.; Höser, S.; Stuhl, F. *J. Chem. Phys.* **1993**, *98*, 7883.

(22) Conway R. R.; Summers, M. E.; Stevens, M. H.; Cardon, J. G.; Preusse, P.; Offermann, D. *Geophys. Res. Lett*. **2000**, *27*, 2613.

(23) Takahashi, K.; Taniguchi, N.; Matsumi, Y.; Kawasaki, M.; Ashfold, M. N. R. *J. Chem. Phys*. **1998**, *108*, 7161.

(24) Denzer, W.; Hancock, G.; Pinot de Moira, J. C.; Tyley, P. L. *Chem. Phys.* **1998**, *231*, 109.

(25) O'Keeffe, P.; Ridley, T.; Lawley, K. P.; Maier, R. R.; Donovan, R. J. *J. Chem. Phys.* **1999**, *110*, 10803.